International Journal of Design & Nature and Ecodynamics
Vol. 21, No. 2, February, 2026, pp. 331-341
Journal homepage: http://iieta.org/journals/ijdne

Non-Destructive Assessment of Internal Wood Conditions Using a Developed Electrical Capacitance Tomography–Dielectric Spectroscopy System

Dyah Ayu Agustiningrum[1,2], Iskandar Zulkarnaen Siregar[3], Ratih Damayanti[4], Warsito Purwo Taruno[5], Lina Karlinasari[1*]

[1] Department of Forest Product, Faculty of Forestry and Environment, IPB University, Bogor 16680, Indonesia
[2] Directorate for Scientific Collection Management, National Research and Innovation Agency (BRIN), Bogor 16911, Indonesia
[3] Department of Silviculture, Faculty of Forestry and Environment, IPB University, Bogor 16680, Indonesia
[4] Directorate for Environment, Maritime, Natural Resources, and Nuclear Policy, National Research and Innovation Agency (BRIN), Jakarta 10340, Indonesia
[5] Center for Non-Destructive Testing and Process Imaging, C-Tech Labs Edwar Technology, Tangerang 15119, Indonesia

Corresponding Author Email: karlinasari@apps.ipb.ac.id

https://doi.org/10.18280/ijdne.210203

Received: 6 December 2025
Revised: 12 February 2026
Accepted: 25 February 2026
Available online: 28 February 2026

Keywords:
Electrical Capacitance Tomography, image analysis, machine learning, tree assessment, internal wood prediction

ABSTRACT

Non-destructive monitoring of internal wood structure is increasingly essential in forest management and timber industries. Conventional methods are often invasive or rely on external symptoms that may not accurately reflect internal decay. This study presents an integrated Electrical Capacitance Tomography and Spectroscopy (ECT-S) system for diagnosing wood log conditions based on their dielectric response across a wide frequency range. A capacitive sensor system was used to measure Sengon wood logs (*Falcataria falcata* (L.) Greuter & R. Rankin) within the frequency range of 250 kHz–60 MHz. Impedance spectra were obtained and analyzed using Principal Component Analysis (PCA) combined with machine learning classifiers to categorize the logs as intact, decayed, or hollow. Cross-sectional images were further examined using ImageJ to validate the internal conditions of each segment. The results show that k-Nearest Neighbors (k-NN) and Random Forest (RF) achieved the highest classification accuracy (0.82). These findings indicate that spectral dielectric characteristics provide useful information for differentiating internal wood conditions and demonstrate the feasibility of integrating tomographic sensing with spectral analysis for nondestructive wood diagnostics. However, the current system remains a prototype and requires further refinement to improve sensitivity and spatial resolution for reliable imaging.

1. INTRODUCTION

Structural abnormalities in trees often manifest as internal defects such as decay and cavities, which are typically caused by biotic agents, including wood-degrading fungi, bacteria, and wood-boring insects such as beetles and termites [1]. Fungal pathogens, particularly those capable of degrading lignin and cellulose, initiate decay by infiltrating the wood and breaking down its primary structural components. This leads to progressive softening of the tissue, discoloration, and a notable decline in mechanical integrity [2-4]. In parallel, termites and similar insect pests contribute to internal cavity formation by excavating extensive tunnels through the heartwood, creating hollow zones within the tree [5]. These internal deteriorations, whether due to microbial decay or insect activity, substantially impair the tree's structural strength and increase its susceptibility to failure, particularly under mechanical or environmental stress.

The evaluation of internal wood conditions is essential for both forest management and the timber industry, as internal defects such as decay, cavities, and structural degradation can significantly reduce wood quality and mechanical performance. Early detection of these defects is therefore crucial to ensure safe utilization and efficient resource management. However, conventional inspection methods are often destructive, time-consuming, or rely heavily on visual inspection of external symptoms, which may not accurately represent the internal condition of wood logs [6, 7].

To address these limitations, various non-destructive evaluation (NDE) techniques have been developed to assess internal wood properties. These include acoustic or stress-wave tomography, X-ray computed tomography, micro-drilling resistance testing, and ground-penetrating radar [8-14]. While these techniques have demonstrated effectiveness in detecting internal defects, some require expensive equipment, complex operational procedures, or limited portability for rapid field inspection.

Electrical and dielectric-based sensing methods have recently emerged as promising alternatives for wood condition monitoring. The dielectric properties of wood are strongly

influenced by factors such as moisture content, density, and internal degradation processes. As a result, dielectric measurements can provide useful information for identifying internal defects and structural heterogeneity. Dielectric spectroscopy, which analyzes the frequency-dependent dielectric response of materials, has been widely used to characterize biological and lignocellulosic materials [15, 16].

Another promising technique is Electrical Capacitance Tomography (ECT), which reconstructs the spatial distribution of permittivity inside an object using capacitance measurements obtained from multiple electrodes surrounding the material without requiring direct contact with the specimen [17-20]. Although ECT has been widely applied in industrial process monitoring, its application in wood diagnostics remains limited. This limitation arises partly from the complex electrical behavior of wood, which is highly anisotropic and strongly influenced by moisture content and internal structural heterogeneity [21, 22]. These factors can cause significant variations in dielectric properties, making the interpretation of capacitance measurements more challenging when using conventional single-frequency ECT approaches.

To address these challenges, integrating ECT with dielectric spectroscopy offers a promising alternative [23]. Spectral measurements across a range of frequencies allow the characterization of the complex permittivity of wood, expressed as:

$$\varepsilon^* = \varepsilon' - j\varepsilon'' \quad (1)$$

where, ε' represents the dielectric constant and ε'' corresponds to dielectric losses [24]. Variations in moisture content, density, and internal degradation processes affect these dielectric parameters differently across frequencies [16]. Therefore, combining tomographic sensing with spectral analysis can provide richer diagnostic information, enabling improved differentiation of internal wood conditions such as intact, decayed, or hollow regions [25].

Based on this concept, this study proposes the development of an integrated Electrical Capacitance Tomography and Spectroscopy (ECT-S) system for evaluating the internal condition of wood logs. The system measures dielectric responses across a wide frequency range (250 kHz–60 MHz), and the resulting impedance spectra are analyzed using Principal Component Analysis (PCA) and machine learning classifiers to distinguish between intact, decayed, and hollow logs.

2. METHODOLOGY

2.1 Data collection

The electrical properties of wood were assessed non-destructively using a capacitance-based measurement system, as described by Oktapiani et al. [26] and Agustiningrum et al. [27]. This system generates static electrical signals across a wide frequency range, from 250 kHz to 60 MHz. A Data Acquisition System (DAS), a Vector Network Analyzer (VNA), and a mini-PC were integrated with a capacitive sensor to conduct the measurements. The sensor consists of parallel copper plates and incorporates a noise suppression mechanism to enhance signal accuracy. As illustrated in Figure 1, the sensor is designed as a flexible belt, allowing it to conform to the curvature of the wood logs for optimal operation.

The sensor system employs a pair of electrodes, comprising a transmitter and a receiver, positioned face-to-face and arranged side-by-side to encircle the perimeter of the wood logs. The systems consist of four channels placed around the circumference of the log. From these four electrodes, six unique electrode pair combinations can be formed (4C2 = 6), allowing multiple electrical signal paths across the cross-section of the log (Figure 2). This configuration enables comprehensive detection of electrical signals across the entire circumference of each log.

Figure 3 presents the full equipment setup, including the sensor installation on the logs. Electrical measurements were conducted along the full length of each log by dividing it into 30 cm segments, corresponding to the width of the sensor.

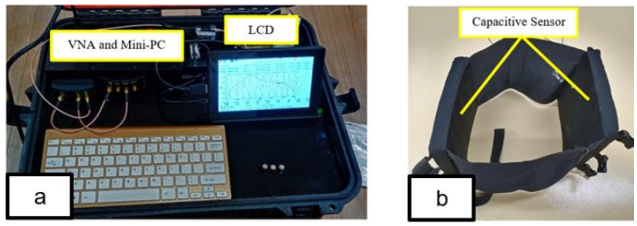

Figure 1. Prototype of ECT-S system (a) DAS component and (b) Belt-shaped capacitive sensor

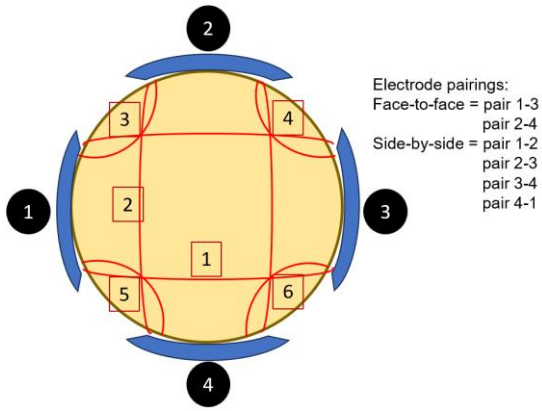

Figure 2. Electrode pairings of a capacitive sensor

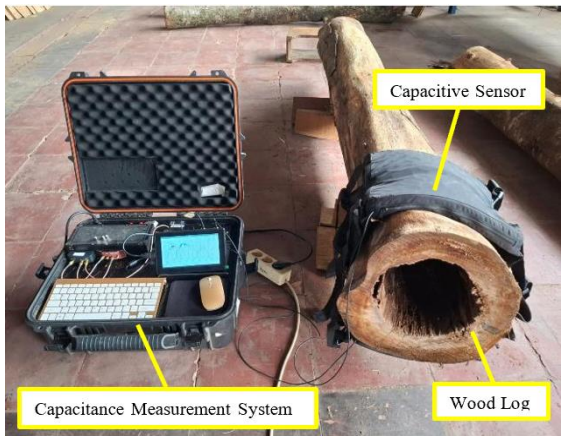

Figure 3. Experimental setup for measuring wood electrical characteristics in a wood log

The sensing electrodes were connected to a VNA to obtain the frequency-dependent electrical response of the sensor–wood system. In this study, measurements were conducted to

determine scattering parameters across a frequency range of 250 kHz–60 MHz. The VNA was configured with a characteristic impedance of 50 Ω, and measurements were recorded for the reflection parameter S_{11} at each frequency point.

The measured S-parameters were converted into complex impedance values using the standard relationship:

$$Z = Z_0 \frac{1 + S_{11}}{1 - S_{11}} \quad (2)$$

where, Z_0 represents the reference impedance of the measurement system (50 Ω) and S_{11} is the measured reflection coefficient. Assuming a predominantly capacitive response, the capacitance values were derived from the imaginary component of the impedance using:

$$C = \frac{-1}{\omega \, \mathrm{Im}(Z)} \quad (3)$$

where, $\omega = 2\pi f$ is the angular frequency and $Im(Z)$ denotes the imaginary part of the impedance. This conversion enables the extraction of frequency-dependent capacitance values from the measured spectral data, which are subsequently used for tomographic sensing and spectral analysis.

The system generates electrical signals that are transmitted from the transmitting (Tx) electrode, propagate through the bark and wood tissues, and are subsequently received by the receiving (Rx) electrode. The resulting signal spectrum is displayed as raw data on an LCD monitor after acquisition. The capacitance measurement system collects electrical property data, which is further processed using machine learning algorithms to extract impedance values corresponding to each measurement point. These impedance responses form the basis for analyzing wood resonance frequencies, in accordance with the methodologies described by van Blokland et al. [28] and Sun [29].

2.2 Image analysis

Image analysis was conducted following non-destructive capacitance-spectroscopy measurements on each 30 cm segment, corresponding to the width of the belt-type sensor. Each wood log was divided into seven segments, as illustrated in Figure 3 (labeled S1–S7), based on its total length. To validate the capacitance-spectroscopy data, transverse cuts were made at the midpoint of each segment, precisely aligned with the sensor's active sensing region, as illustrated in Figure 4 (red dashed line). The resulting wood cross-sections were photographed to obtain high-resolution images that revealed the internal structure. These images were analyzed to identify structural defects, including both hollow and decay regions. ImageJ software was employed to detect and delineate abnormal areas, which were then quantified. The extent of deterioration was determined by calculating the percentage of the defective area relative to the total cross-sectional area for each segment.

Wood cross-sections were classified as decayed when they exhibited tissue softening accompanied by dark discoloration and observable alterations in fiber structure relative to intact wood. Hollow conditions were defined by the complete loss of wood tissue, resulting in a visible cavity, typically located at the center of the cross-section. These structural anomalies were identified through visual examination of cross-sectional images prior to classification. The proportions of decay and hollow areas, calculated as percentages of the total cross-sectional area, were subsequently used to validate the electrical measurements obtained from the ECT-S system.

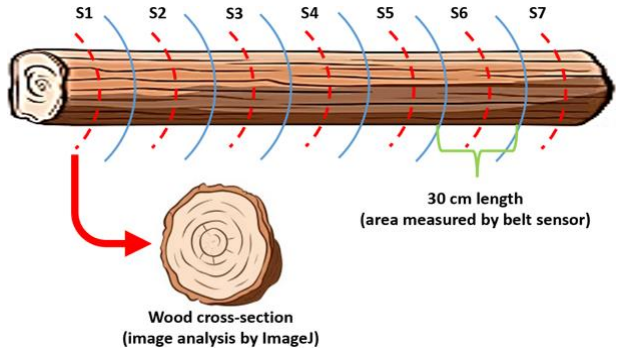

Figure 4. Illustration of segment cuts on the wood log and the segment cross-sections

2.3 Data analysis

The measured electrical response of each wood sample was represented by its frequency-dependent impedance spectrum obtained across the measurement range of 250 kHz–60 MHz. Instead of using a single-frequency measurement, the complete spectral response was used to capture variations in the dielectric behavior of the samples.

For each measurement, the impedance values recorded at discrete frequency points were arranged into a feature vector representing the spectral electrical characteristics of the sample. These spectral vectors contain information about changes in capacitance and dielectric losses that may arise from internal structural variations such as decay or cavities.

Since the spectral dataset contains a large number of frequency points, PCA was applied to reduce the dimensionality of the feature space while preserving the dominant variance in the data. PCA transforms the original spectral vectors into a smaller set of orthogonal principal components that represent the most significant patterns in the impedance spectra.

The resulting principal component scores were then used as input features for machine learning classifiers to distinguish between intact, decayed, and hollow wood logs. In this study, classification models including Support Vector Machine (SVM), k-Nearest Neighbors (k-NN), and Random Forest (RF) were implemented to evaluate the discriminative capability of the spectral dielectric signatures [30].

3. RESULTS AND DISCUSSION

3.1 Impedance patterns and resonance behavior of wood logs

The capacitance-based measurement system produced raw complex data from the wood logs, primarily composed of imaginary components. As a result, data extraction procedures were necessary to calculate impedance, resistance, and capacitance values across the frequency range of 250 kHz–60 MHz. Subsequent analysis centered on identifying resonance behavior, which consistently manifested as a pronounced increase in impedance within the 17–30 MHz range (Figure 5), while lower impedance values were observed outside this

band. Notably, the raw dataset included both outliers and missing values, likely introduced by measurement inaccuracies related to environmental influences, sensor limitations, or system noise. Therefore, data preprocessing, comprising outlier detection and imputation of missing values, was essential to ensure the integrity of the measurements and to accurately represent the material's dielectric polarization in response to the applied electric field [31].

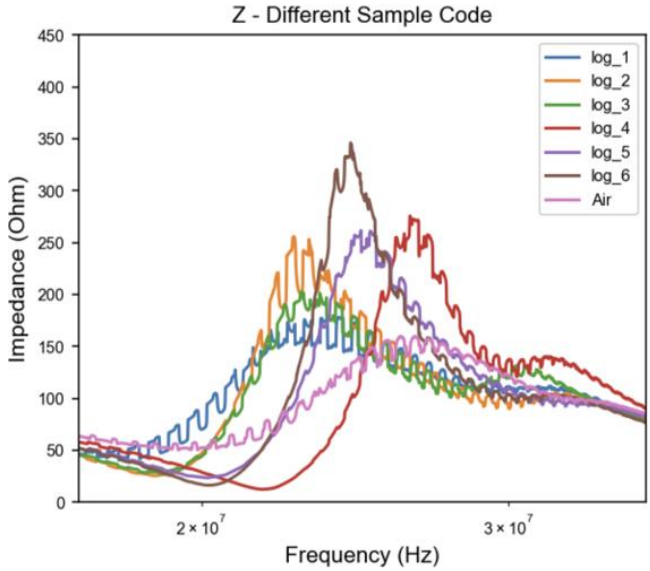

Figure 5. Impedance graphic of wood logs compared with air

The analysis focused on the resonance frequency range, where peak impedance values were used to assess the wood's dielectric response. The results revealed clear distinctions between different wood conditions. Intact segments consistently showed the highest impedance peaks, indicating strong dielectric polarization, while hollow sections produced values that were very close to those of air, suggesting minimal interaction with the electric field. In this context, air was used as a baseline reference because of its low relative permittivity, approximately 1, in contrast to dry wood (which typically ranges from 2 to 4) and wet wood, which can exceed 20 due to its higher water content [24, 32, 33]. These findings highlight how the dielectric response can reflect underlying structural integrity, making it a useful indicator for assessing internal wood conditions.

The impedance spectra of the six wood logs, along with air as a reference standard, revealed distinct clustering patterns (Figure 5). Log 6 fell within a high-impedance cluster, characteristic of intact wood exhibiting strong resonance behavior. In contrast, Logs 4 and 5 formed a mid-impedance cluster, with downward-shifted peaks, suggesting the presence of mild to moderate decay or small internal voids. Meanwhile, Logs 1, 2, and 3, along with the air reference, were grouped into a low-impedance cluster, marked by flat spectral profiles. These curves closely approached the air baseline, consistent with the behavior expected from hollow or severely deteriorated wood, or loosely packed material with minimal dielectric response.

Although all specimens exhibited resonance within the 17–30 MHz range, the location of the resonance peaks varied. Shifts to higher frequencies were generally associated with denser or drier wood, while shifts to lower frequencies appeared to correlate with higher moisture content or structural degradation. Notably, the similar spectral profiles observed in the decay logs (Logs 4 and 5) suggest that a single impedance spectrum may not be sufficient to distinguish between different stages or types of decay. This highlights the potential benefit of applying multivariate analysis techniques, such as PCA or clustering algorithms, to better classify and interpret wood decay characteristics across a spectrum of conditions. The air spectrum serves effectively as a control, representing the lower bound of permittivity and impedance response, and is clearly separated from all wood samples.

Figure 6 presents the impedance magnitude spectra for each individual log segment, highlighting the frequency-dependent electrical behavior across varying internal conditions. The intact logs (e.g., Log 4, Log 6) consistently show high and stable impedance in the 17–30 MHz range, with gradual slopes and minimal fluctuations. These smooth profiles are characteristic of dielectric continuity, reflecting structurally sound wood with evenly distributed moisture and intact cellular architecture. The impedance peaks correspond to high capacitive opposition to current flow, as expected in solid and homogenous dielectric media.

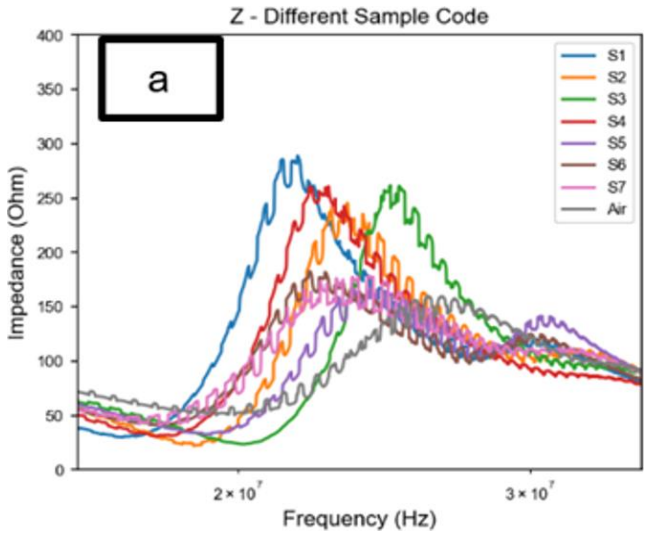

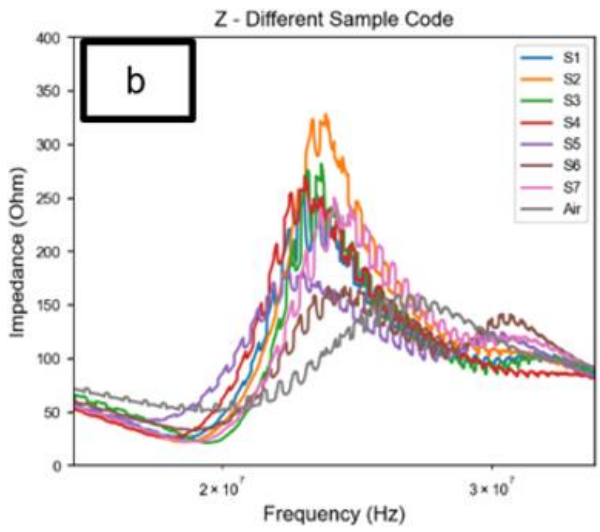

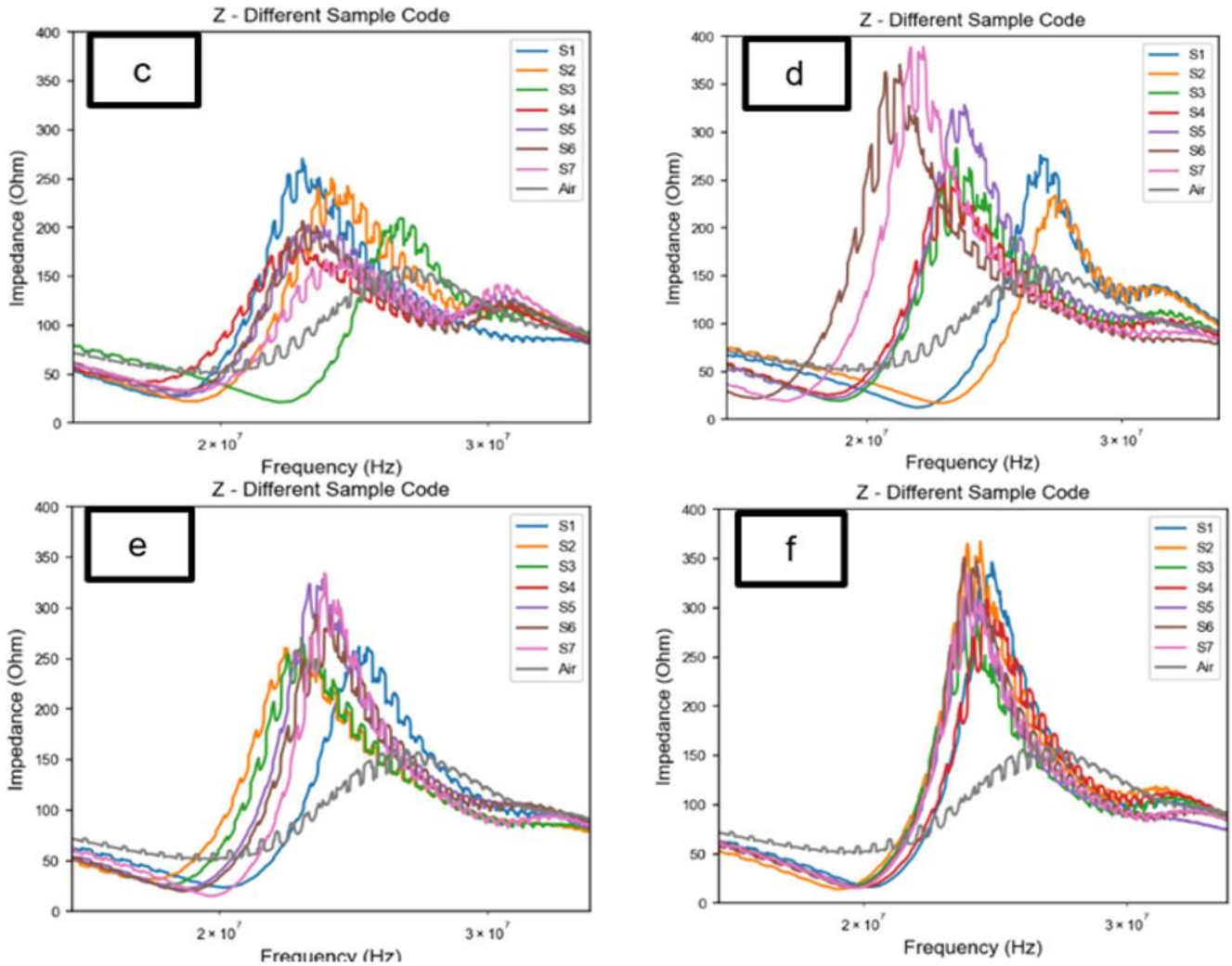

Figure 6. Impedance graphic of each log and segment compared with air as reference (a) Log 1, (b) Log 2, (c) Log 3, (d) Log 4, (e) Log 5, and (f) Log 6

In contrast, hollow logs (e.g., Log 1, Log 3) display significantly lower impedance magnitudes across the entire spectrum. This reduction is especially evident in the high-frequency region (above 25 MHz), where impedance curves flatten and show a complete absence of resonance features. This behavior indicates the dominance of air-filled voids, which reduce the effective relative permittivity and disrupt internal capacitive networks. The lack of clear spectral transitions suggests limited field interaction with solid wood material, in line with severe structural loss.

Decay-affected logs (e.g., Log 2, Log 5) demonstrate intermediate impedance behavior, with irregular curve shapes and localized dips in the 20–30 MHz band. These features may represent partial resonance effects resulting from decayed tissues acting as lossy, inhomogeneous dielectrics. The presence of fluctuating impedance gradients implies heterogeneous moisture content and breakdown of wall-bound water retention in partially degraded wood regions. In several cases, a mild resonance signature appears near 23–27 MHz, possibly caused by cavity-like geometries formed during mid-stage degradation.

Taken together, the spectral profiles in Figure 6 provide a diagnostic basis for distinguishing between wood conditions through their dielectric signatures. The resonance behavior observed in decayed samples, the damping of impedance in hollow logs, and the preserved permittivity in intact wood support the feasibility of frequency-based feature extraction. These distinctions justify the application of PCA and supervised classifiers in subsequent sections.

Interestingly, a deviation from the theoretical relationship between electrical impedance and permittivity was observed. According to the fundamental equation below [24]:

$$Z = \frac{1}{j\omega\varepsilon_0\varepsilon_r A / d} \tag{4}$$

where, Z is the electrical impedance, j is the imaginary unit, ω is the angular frequency of the AC signal, ε_0 is the permittivity of free space, ε_r is the relative permittivity, A is the area of the electrodes facing each other, and d is the distance between the electrodes.

It is commonly expected that impedance decreases as permittivity increases. Following this logic, one might assume that air-filled cavities, with their inherently low permittivity, would exhibit higher impedance values. While this reasoning is sound in a static context, experimental observations showed that hollow regions frequently produced lower impedance values. This apparent contradiction is explained by the influence of high-frequency resonance effects and dielectric loss mechanisms. As noted by Torgovnikov [24], dielectric resonance phenomena become particularly prominent at frequencies above 10 MHz and can significantly alter impedance behavior. Therefore, the sharp reductions in

impedance observed at specific frequencies are not anomalies, but anticipated outcomes of these effects.

Additionally, dielectric loss plays a critical role in the energy dissipation process. It represents the portion of the electric field energy lost as heat, particularly in materials with polar molecules. Segments of wood that are dense, moisture-rich, or structurally intact typically exhibit higher dielectric loss due to dipolar relaxation involving both water molecules and the wood's structural polymers (e.g., cellulose and lignin). This contributes to increased permittivity and correspondingly higher impedance. In contrast, air-filled cavities lack the molecular structure necessary to absorb and dissipate energy effectively, particularly at higher frequencies, resulting in a net decrease in impedance values [34-36].

These interpretations are further supported by the observed impedance behavior across the frequency spectrum. Notably, wood logs containing internal defects exhibited higher impedance than intact samples at lower frequencies (< 10 MHz). However, as the frequency increased, particularly within the 17–30 MHz range, a pronounced drop in impedance was observed. This behavior is consistent with known dielectric resonance and energy loss mechanisms, where structural degradation alters how the material interacts with the applied electric field. Such frequency-dependent patterns provide valuable diagnostic signatures, making them particularly suitable for spectroscopic classification and enabling differentiation of internal wood conditions with greater precision.

3.2 Image analysis results

Each log segment was evaluated using cross-sectional image analysis to identify internal defects, including regions of decay and hollowness. Defects were visually distinguished based on observable changes in texture, discoloration, and the presence of voids within the wood structure. These areas were then delineated as defective zones. The extent of deterioration was quantified using an areal ratio, defined as the area of the defect divided by the total cross-sectional area of the corresponding segment. Representative images of each segment, along with the visually identified defect zones, are provided in Table 1. Meanwhile, the quantitative results of the abnormal area ratio for each log segment, determined through ImageJ analysis, are summarized in Table 2.

This investigation confirms the capability of the developed capacitance-based electrical measurement system to non-invasively distinguish between intact, decayed, and hollow wood based on their respective dielectric responses. In particular, resonance frequency analysis within the 17–30 MHz range proved effective in identifying structural variations, with solid and homogeneous wood samples exhibiting sharper impedance peaks compared to more heterogeneous or degraded specimens. However, the system demonstrated limited sensitivity in distinguishing the severity of decay, suggesting room for improvement in detecting intermediate stages of degradation. To enhance the diagnostic performance of this approach, future studies are encouraged to adopt more controlled experimental conditions and to comprehensively characterize wood properties, such as moisture content, density, and mechanical strength. These efforts would help clarify the extent to which each variable influences the electrical behavior of wood and support more accurate, non-destructive assessment of internal structural integrity.

For Logs 4 to 6, external visual inspection initially suggested that all three were structurally sound, as their outer surfaces appeared intact and free from visible defects. However, upon cross-sectional examination, performed at intervals beginning 15 cm from each end, internal irregularities were detected as early as the first segment.

In Log 4, central degradation was identified in segments L4S1 to L4S3. Although some softwood fibers were still present externally, suggesting partial integrity, the internal condition was compromised. Conversely, segments L4S4 to L4S7 displayed visually sound characteristics, with no obvious signs of internal decomposition, indicating that deterioration was localized toward one end of the log.

Table 1. Picture of cross-section from each segment and log

Segment Code	L1	L2	L3	L4	L5	L6
S1						
S2						
S3						

Segment Code	L1	L2	L3	L4	L5	L6
S4						
S5						
S6						
S7						

Table 2. Ratio of abnormal area in wood cross-sections per log and segment from ImageJ analysis

	Segment 1	Segment 2	Segment 3	Segment 4	Segment 5	Segment 6	Segment 7
Log 1							
Hollow (%)	7.34	10.00	14.16	11.62	15.98	13.50	12.18
Decay (%)	-	-	17.92	19.12	20.00	29.72	34.24
Log 2							
Hollow (%)	-	0.45	-	-	19.53	25.20	29.59
Decay (%)	19.98	37.10	47.22	36.92	33.34	14.66	10.16
Log 3							
Hollow (%)	4.47	9.88	17.86	14.17	19.94	22.64	31.07
Decay (%)	43.85	37.39	33.12	31.66	18.09	17.19	8.90
Log 4							
Hollow (%)	-	-	-	-	-	-	-
Decay (%)	20.02	17.60	-	-	2.92	-	-
Log 5							
Hollow (%)	17.18	8.76	-	2.82	-	-	-
Decay (%)	21.77	27.84	31.68	23.18	-	-	-
Log 6							
Hollow (%)	4.46	2.93	3.26	3.16	-	-	-
Decay (%)	-	-	-	-	-	-	-

Log 5 revealed more extensive internal damage. Segments L5S1 through L5S4 showed significant decay, including localized hollow zones and marked structural compromise. In contrast, segments L5S5 and L5S6 appeared relatively intact, with no visual signs of degradation. Segment L5S7, while structurally intact on visual inspection, exhibited a distinct blackish discoloration, likely indicative of fungal activity. As the sectioning progressed, additional signs of internal cracking and fragmentation emerged, revealing levels of decay not apparent from the external assessment.

In Log 6, small internal voids were present in segments L6S1 through L6S4, suggesting the onset of cavity formation. Segments L6S5 through L6S7, however, showed no visible anomalies or signs of structural failure. These findings underscore the limitations of relying solely on external inspection to evaluate wood quality. The discrepancies between visual appearance and internal condition highlight the importance of employing non-destructive testing methods to assess the true structural integrity of wood.

3.3 Principal Component Analysis and classification

To explore patterns in the data, PCA was applied to the capacitance features. The resulting scatter matrix (Figure 7) displays the distribution of samples across the first four principal components (PC1–PC4). PC1 effectively separates air samples (blue) from all wood categories (Intact, Decay, and Hollow), highlighting the clear dielectric contrast between air and wood. This strong separation confirms that the ECT-S system is highly sensitive to differences in dielectric properties.

Further differentiation is visible in PC2 and PC3, which reveal partial clustering among the wood categories. Hollow (green) and Intact (red) samples begin to diverge in the PC2–

PC3 space, whereas Decay (orange) samples overlap with both. This overlap reflects the complex and gradual nature of wood degradation. Notably, the separation of Hollow and Intact samples suggests that differences in material density and dielectric storage capacity are effectively captured through these principal components.

While PC4 contributes less to the total variance and exhibits greater class overlap, its inclusion alongside PC1–PC3 adds to the multidimensional representation of wood structure. Together, these components form a comprehensive framework for clustering and classification tasks, enhancing interpretability in structural diagnosis.

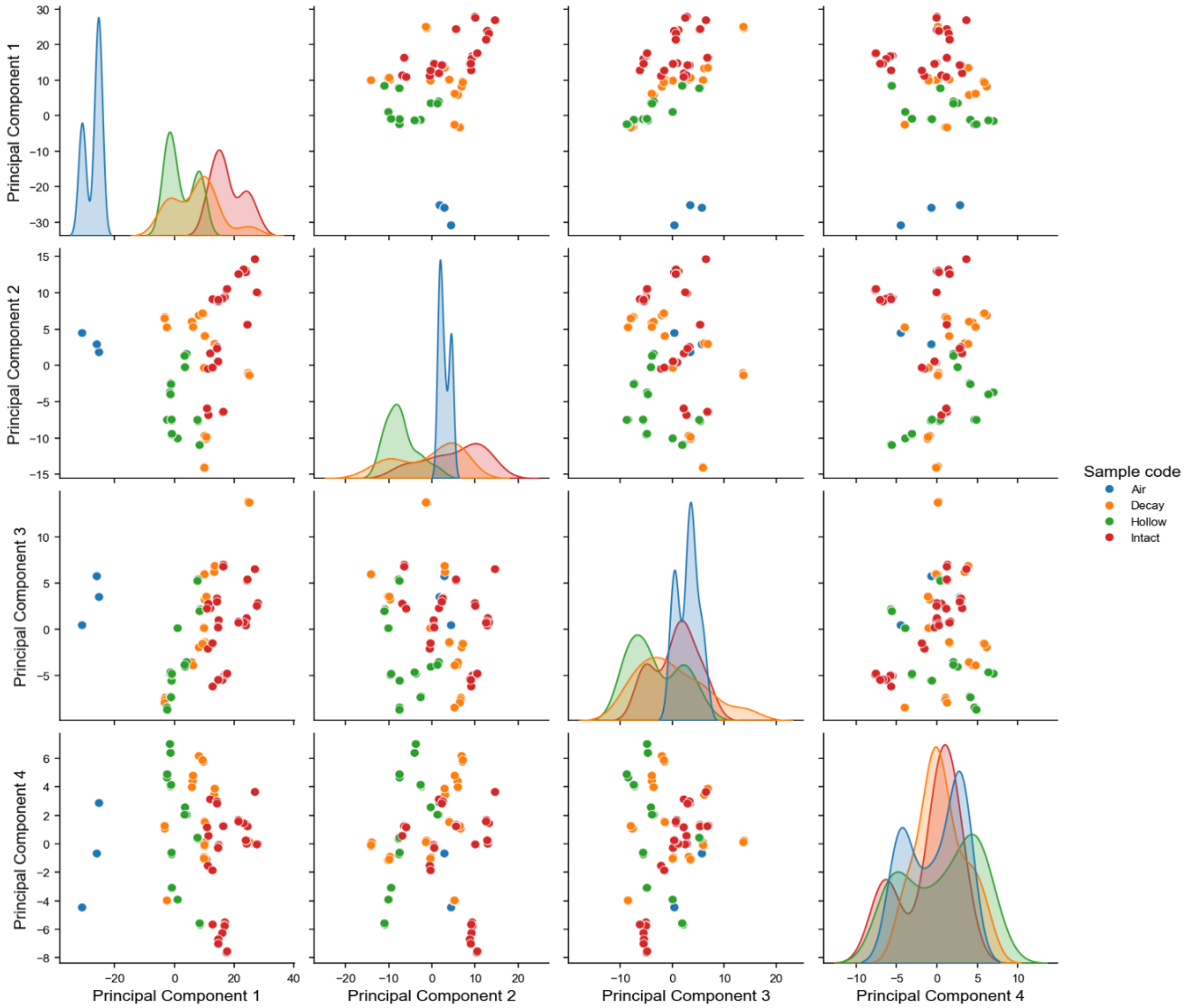

Figure 7. Principal Component Analysis (PCA) plotting of the capacitance value of wood logs in various conditions

3.4 Classification performance diagnostic reliability

Three classification algorithms, namely SVM, k-NN, and RF, were implemented to assess their ability to differentiate among Intact, Decay, and Hollow wood categories. Each model was trained on 80% of the data and tested on the remaining 20% using stratified sampling to ensure balanced class representation. Input features consisted of the first three principal components (PC1–PC3), which were sufficient to retain the essential structure of the data. Model performance was evaluated through accuracy, precision, recall, and F1-score metrics, supported by confusion matrix analysis. Among the classifiers, the k-NN and RF models demonstrated higher accuracy than SVM (Table 3).

Among the models, SVM yielded the lowest overall accuracy (77%), primarily due to its poor recall for the decay class (0.29). A substantial number of decay samples were misclassified as hollow, indicating difficulty in delineating the subtle transition between partially and severely degraded wood. Nevertheless, SVM performed well in identifying Intact samples with perfect recall and high precision, suggesting that this class presents clearer dielectric separation in the feature space. In contrast, both k-NN and RF achieved higher classification accuracy, each reaching 82%. The k-NN model demonstrated balanced recall across all classes, particularly in detecting decay (0.71) and hollow (0.86). The RF model also performed reliably, with slightly lower consistency between decay and hollow classifications (both with 0.71 recall), but with perfect precision and recall for intact samples. This indicates that while decision boundaries between degraded wood types may remain challenging, ensemble-based classifiers such as RF can still provide robust performance for more well-defined categories. The confusion matrix of k-NN and RF is presented in Figure 8.

Table 3. Summary of classification performance based on Principal Component Analysis (PCA) features

Classifier	Accuracy	Macro Precision	Macro Recall	Macro F1-Score	Remarks
Support Vector Machine (SVM)	0.77	0.84	0.76	0.72	Lower recall for the decay class indicates difficulty in distinguishing overlapping patterns.
k-Nearest Neighbors (k-NN)	0.82	0.82	0.82	0.82	Highest overall performance, all classes classified with high precision and recall.
Random Forest (RF)	0.82	0.81	0.81	0.81	High overall performance, all classes classified with high precision and recall.

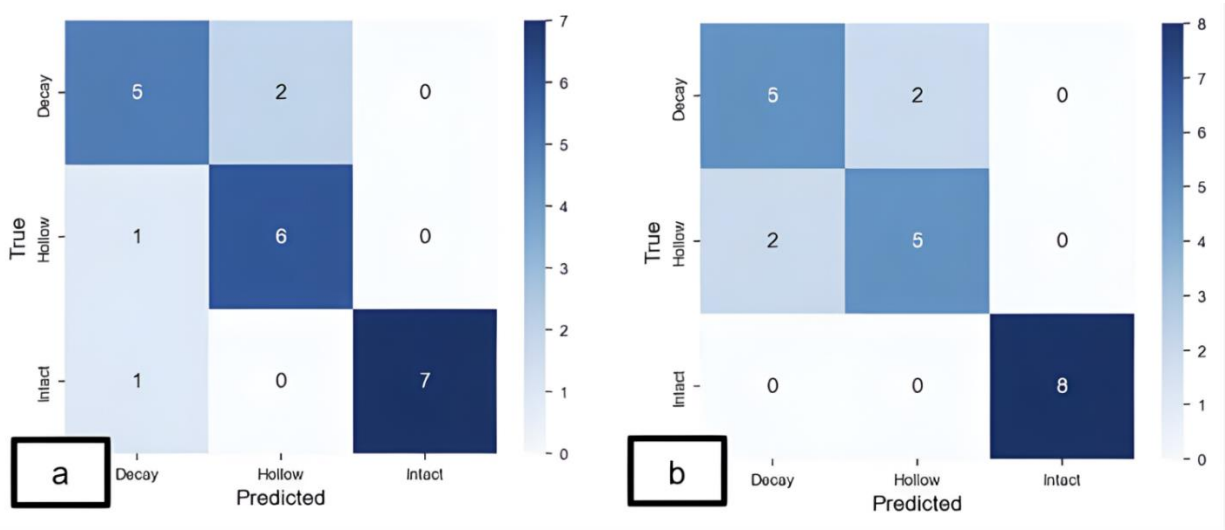

Figure 8. Confusion matrix of (a) k-NN and (b) Random Forest (RF)

In Figure 8(a), the k-NN model correctly identified 5 out of 7 decay samples, while misclassifying 2 as hollow. Similarly, it correctly classified 6 hollow samples, with one misclassified as decay. All but one intact sample was correctly predicted, indicating strong model sensitivity to undamaged wood, though with a slight overlap toward the decay class.

Figure 8(b) shows the performance of the RF classifier, which also correctly classified 5 decay samples and 5 hollow samples. However, it misclassified two hollow samples as decay, indicating a slight shift in confusion direction compared to k-NN. Notably, all intact samples were classified with perfect accuracy, demonstrating RF's ability to robustly separate this class. Although the recall for hollow was slightly lower than that of k-NN, the complete absence of errors in the intact category supports the overall strength of ensemble-based classification in identifying clearly defined wood conditions.

3.5 Electrical Capacitance Tomography–Spectroscopy system performance

The flexible capacitive sensor platform, featuring parallel copper electrodes, performed reliably across a range of wood diameters. Its belt-shaped design allowed conformal attachment to wood surfaces, while internal damping mechanisms helped reduce signal noise. The system produced consistent signal responses within the frequency range of 250 kHz to 60 MHz, with distinct resonance behavior typically observed between 17 and 30 MHz.

Despite its effectiveness, the system presented some limitations. The spatial resolution was constrained by the 30 cm segment size, which may limit the detection of small or localized defects. Additionally, signal accuracy could be affected by environmental noise and sensor-to-log contact variability, particularly in field conditions. These issues suggest that improvements in sensor calibration, shielding, and mechanical design are needed to enhance robustness. While the ECT-S system demonstrated high sensitivity for detecting general internal defects, it still faces challenges in resolving intermediate levels of decay, where impedance patterns tend to overlap. The complex interplay of moisture content, density variation, and structural heterogeneity complicates straightforward classification.

4. CONCLUSIONS

The results of this study provide an initial demonstration of the feasibility of integrating tomographic sensing with spectral dielectric analysis as a non-destructive diagnostic approach for assessing internal wood conditions. The developed ECT-S system enables the detection of internal abnormalities through profiling of dielectric properties. The integration of spectral measurements with Principal Component Analysis (PCA) and supervised learning methods further enhances its capability to differentiate wood conditions based on their dielectric signatures. However, the current system remains a prototype under development. Further improvements in sensing resolution and advanced data analysis are required to enhance detection accuracy and to better characterize different stages of wood decay.

ACKNOWLEDGMENT

The authors are grateful to the Ministry of Education, Culture, Research, and Technology (KEMENDIKBUDRISTEK) and IPB University for the

assistance and funding provided through the Doctoral Dissertation Research Grant for the Fiscal Year 2024. Furthermore, the authors are grateful to IPB University and the National Research and Innovation Agency (BRIN) Team for the assistance rendered with the field and laboratory work.

REFERENCES

[1] Mattheck, C., Breloer, H. (1994). The Body Language of Trees: A Handbook for Failure Analysis. HMSO Publisher.

[2] Papandrea, S.F., Cataldo, M.F., Zimbalatti, G., Proto, A.R. (2022). Comparative evaluation of inspection techniques for decay detection in urban trees. Sensors and Actuators A: Physical, 340: 113544. https://doi.org/10.1016/j.sna.2022.113544

[3] Pearce, R.B. (2000). Decay development and its restriction in trees. Journal of Arboriculture, 26(1): 1-11. https://doi.org/10.48044/jauf.2000.001

[4] Soge, A.O., Popoola, O.I., Adetoyinbo, A.A. (2021). Detection of wood decay and cavities in living trees: A review. Canadian Journal of Forest Research, 51(7): 937-947. https://doi.org/10.1139/cjfr-2020-0340

[5] Nandika, D., Karlinasari, L., Siregar, I.Z., Lestari, A.T., Nababan, M.Y.S. (2018). Characteristics of exposed cavities of urban trees in a landscape of Southern Jakarta and their filling using polyurethane foam. IOP Conference Series: Earth and Environmental Science, 203(1): 012029. https://doi.org/10.1088/1755-1315/203/1/012029

[6] Pratiwi, L., and Safe'i, R. (2018). Teak tree vitality assessment with forest health monitoring at KPH Balapulang. Ecogreen, 4(1): 9-15. https://ojs.uho.ac.id/index.php/green/article/view/4156/3232.

[7] Azzi, Z., Al Sayegh, H., Metwally, O., and Eissa, M. (2025). Review of nondestructive testing (NDT) techniques for timber structures. Infrastructures, 10(2): 28. https://doi.org/10.3390/infrastructures10020028

[8] Espinosa, L., Arciniegas, A., Cortes, Y., Prieto, F., Brancheriau, L. (2017). Automatic segmentation of acoustic tomography images for the measurement of wood decay. Wood Science and Technology, 51(1): 69-84. https://doi.org/10.1007/s00226-016-0878-1

[9] Gao, S., Wang, X., Wiemann, M.C., Brashaw, B.K., Ross, R.J., Wang, L. (2017). A critical analysis of methods for rapid and nondestructive determination of wood density in standing trees. Annals of Forest Science, 74(2): 27. https://doi.org/10.1007/s13595-017-0623-4

[10] Li, H., Zhang, X., Li, Z., Wen, J., Tan, X. (2022). A review of research on tree risk assessment methods. Forests, 13(10): 1556. https://doi.org/10.3390/f13101556

[11] Nicolotti, G., Socco, L.V., Martinis, R., Godio, A., Sambuelli, L. (2003). Application and comparison of three tomographic techniques for detection of decay in trees. Arboriculture & Urban Forestry, 29(2): 66-78. https://doi.org/10.48044/jauf.2003.009

[12] So, C.L., Via, B.K., Groom, L.H., Schimleck, L.R., Shupe, T.F., Kelley, S.S., Rials, T.G. (2004). Near infrared spectroscopy in the forest products industry. Forest Products Journal, 54(3): 6-16. https://www.srs.fs.usda.gov/pubs/ja/ja_so001.pdf.

[13] Vössing, K.J., Niederleithinger, E. (2018). Nondestructive assessment and imaging methods for internal inspection of timber: A review. Holzforschung, 72(6): 467-476. https://doi.org/10.1515/hf-2017-0122

[14] Singh, K.P., Siregar, I.Z., Abad, J.I.M., and Karlinasari, L. (2022). Non-destructive modeling using a drilling resistance tool to predict wood basic density of standing trees in a eucalyptus plantation in North Sumatra, Indonesia. Biodiversitas, 23(12): 6218-6226. https://doi.org/10.13057/biodiv/d231217

[15] Skierucha, W., Wilczek, A., and Szypłowska, A. (2012). Dielectric spectroscopy in agrophysics. International Agrophysics, 26: 187-197. https://doi.org/10.2478/v10247-012-0027-5

[16] Khaled, D.E., Castellano, N.N., Gázquez, J.A., Perea-Moreno, A.J., Manzano-Agugliaro, F. (2016). Dielectric spectroscopy in biomaterials: Agrophysics. Materials, 3: 310. https://doi.org/10.3390/ma9050310

[17] Warsito, W., Marashdeh, Q., Fan, L.S. (2007). Electrical capacitance volume tomography (ECVT). IEEE Sensors Journal, 7(4): 525-535. https://doi.org/10.1109/JSEN.2007.891952

[18] Baidillah, M., Warsito, W., Mukhlisin, M. (2011). The optimum design of 3D sensor for electrical capacitance volume-tomography (ECVT). Jurnal Matematika dan Sains, 16(3): 123-128. https://www.researchgate.net/publication/303658624_The_Optimum_Design_of_3D_Sensor_for_Electrical_Capacitance_Volume-Tomography_ECVT.

[19] Carcangiu, S., Fanni, A., Montisci, A. (2019). Electric capacitance tomography for nondestructive testing of standing trees. International Journal of Numerical Modelling: Electronic Networks, Devices and Fields, 32(4): e2252. https://doi.org/10.1002/jnm.2252

[20] Esofita, M., Djamal, M., Taruno, W.P., Al Huda, M., Baidillah, M., Pari, G., Damayanti, R. (2015). Analysis of wood's capacitance characteristic to its hardness. Applied Mechanics and Materials, 771: 161-164. https://doi.org/10.4028/www.scientific.net/AMM.771.161

[21] Amato, M.T., Subroy, V., Giménez, D., Strom, P.F., Krogmann, U. (2019). Dielectric permittivity-water content relationships in woodchips: Particle size and temperature effects. Journal of Hydrology, 572: 251-260. https://doi.org/10.1016/j.jhydrol.2019.02.047

[22] Razafindratsima, S., Sbartai, Z.M., Demontoux, F. (2017). Permittivity measurement of wood material over a wide range of moisture content. Wood Science and Technology, 51: 1421-1431. https://doi.org/10.1007/s00226-017-0935-4

[23] Marashdeh, Q., Warsito, W., Fan, L.S., and Teixeira, F.L. (2007). A multimodal tomography system based on ECT sensors. IEEE Sensors Journal, 7(3): 426-433. https://doi.org/10.1109/JSEN.2006.890149

[24] Torgovnikov, G.I. (1993). Dielectric Properties of Wood and Wood-Based Materials. Springer Berlin, Heidelberg. https://doi.org/10.1007/978-3-642-77453-9

[25] Ismail, I., Gamio J.C., Bukhari, S.F.A., Yang W.Q. (2005). Tomography for multi-phase flow measurement in the oil industry. Flow Measurement and Instrumentation, 16(2): 145-155. https://doi.org/10.1016/j.flowmeasinst.2005.02.017

[26] Oktapiani, C., Damayanti, R., Karlinasari, L., Agustiningrum, D.A., et al. (2025). The effect of

anatomical structure on hygroscopicity of four wood species. AIP Conference Proceedings, 3172(1): 020039. https://doi.org/10.1063/5.0249377

[27] Agustiningrum, D.A., Siregar, I.Z., Damayanti, R., Taruno, W.P., Nugraha, H., Rohmadi, Karlinasari, L. (2024). Electrical properties at multi-frequencies for analysis of physical and anatomical properties of fast-growing standing teak trees at various ages. Forests, 15(4): 669. https://doi.org/10.3390/f15040669

[28] van Blokland, J., Nasir, V., Cool, J., Avramidis, S., Adamopoulos, S. (2021). Machine learning-based prediction of surface checks and bending properties in weathered thermally modified timber. Construction and Building Materials, 307: 124996. https://doi.org/10.1016/j.conbuildmat.2021.124996

[29] Sun, P.A. (2022). Wood quality defect detection based on deep learning and multicriteria framework. Mathematical Problems in Engineering, 2022(1): 4878090. https://doi.org/10.1155/2022/4878090

[30] Król, K., Rymarczyk, T., Kozłowski, E., Niderla, K. (2022). Using principal component analysis and elastic net in logistic regression to identify the location of objects in EIT. Journal of Physics: Conference Series, 2408(1): 012025. https://doi.org/10.1088/1742-6596/2408/1/012025

[31] Guo, Z.H. (2011). New normalization method of imaging data for electrical capacitance tomography. In 2011 International Conference on Mechatronic Science, Electric Engineering and Computer (MEC), Jilin, China, pp. 1126-1130. https://doi.org/10.1109/MEC.2011.6025665

[32] Artagan, S.S., Borecky, V. (2015). Applicability of GPR on Turkish railways. https://www.researchgate.net/publication/294848218_Applicability_of_GPR_on_Turkish_Railways.

[33] Gadonna, K., Leroy, O., Leprince, P., Alves, L.L., Boisse-Laporte, C. (2012). Study of gas heating by a microwave plasma torch. Journal of Modern Physics, 3(10): 1603-1615. http://doi.org/10.4236/jmp.2012.330198

[34] Ghildiyal, V., Altaner, C.M., Heffernan, B., Jarvis, M.C. (2025). Electrical phenomena in trees and wood: A review. Current Forestry Reports, 11(1): 7. https://doi.org/10.1007/s40725-024-00238-0

[35] Raatevaara, A., Korpunen, H., Tiitta, M., Tomppo, L., Kulju, S., Antikainen, J., Uusitalo, J. (2020). Electrical impedance and image analysis methods in detecting and measuring Scots pine heartwood from a log end during tree harvesting. Computers and Electronics in Agriculture, 177: 105690. https://doi.org/10.1016/j.compag.2020.105690

[36] Eric, N.A., Samuel, E., Jacques, M., Serge, D.Y., Vuong, T.P. (2024). Measurement of the dielectric properties of tropical wood species for application to millimetre-band antennas. Material Design & Processing Communications, 2024(1): 7777701. https://doi.org/10.1155/2024/7777701